Journal of Power Sources 226 (2013) 122–126

Contents lists available at SciVerse ScienceDirect

Journal of Power Sources

journal homepage: www.elsevier.com/locate/jpowsour

Short communication

Analysis of the size effect of $LiMnPO_4$ particles on the battery properties by using STEM-EELS

J. Yoshida [a,*], M. Stark [b], J. Holzbock [b], N. Hüsing [c], S. Nakanishi [a], H. Iba [a], H. Abe [d], M. Naito [d]

[a] Battery Research Division, Toyota Motor Corporation, 1200, Mishuku, Susono, Shizuoka 410-1193, Japan
[b] Institut für Anorganische Chemie I, Ulm University, Albert-Einstein-Allee 11, 89081 Ulm, Germany
[c] Materials Chemistry, Paris-Lodron University Salzburg, Hellbrunner Str. 34, A-5020 Salzburg, Austria
[d] Joining and Welding Research Institute, Osaka University, 11-1, Mihogaoka, Ibaraki, Osaka 567-0047, Japan

HIGHLIGHTS

- Different sizes of $LiMnPO_4$ particles were synthesized by two synthesis methods.
- The size effect of the $LiMnPO_4$ particles on the battery was revealed by EELS.
- The particle which sizes less than 40 nm exhibited the high rate performance.

ARTICLE INFO

Article history:
Received 11 July 2012
Received in revised form
18 September 2012
Accepted 21 September 2012
Available online 26 October 2012

Keywords:
Li-ion battery
Cathode
Olivine
Nano particle
EELS

ABSTRACT

The $LiMnPO_4$ cathode material is a good candidate for rechargeable lithium ion batteries because of high voltage (4.1 V), high thermal stability and no toxicity. However, the rate performance of this material is extremely low when compared to the conventional $LiMO_2$ (M = Ni or Co) or $LiFePO_4$. In this study, the primary particle size was reduced by a hydrothermal synthesis, and we obtained $LiMnPO_4$ particles with sizes less than 40 nm. The sample exhibited an excellent rate capacity, which was 136 mAh g^{-1} at 5 C and 120 mAh g^{-1} at 10 C. We also revealed the effect of the $LiMnPO_4$ particle size on the battery by introducing STEM-EELS, which was expected to allow for the direct microscopic observation of the lithium state in the particles during the charge-discharge process. With the EELS analysis, it was clarified that the lithium diffusion distance from the inside to the surface of the primary particles had to be reduced down to about 20 nm to achieve the high rate performance.

1. Introduction

$LiMPO_4$ (M = Fe, Mn) has been intensively studied as one of the future cathode materials for lithium ion batteries since Padhi et al.'s report [1] in 1997. Especially, $LiMnPO_4$ is expected to be an alternative to layer structured materials, such as $LiCoO_2$ or $LiNiO_2$, already being used for commercialized batteries, because $LiMnPO_4$ has a higher voltage (4.1 V) than the layer structured materials. In addition, it exhibits a higher thermal stability due to the covalent bonds between the oxygen and phosphorus in the polyanion part (PO_4). However, the main drawback of $LiMnPO_4$ is the extreme difficulty of the lithium insertion/extraction reaction compared to $LiFePO_4$ because of its poor lithium ion diffusion and electron conductivity [2–6]. The electron conductive mechanism of $LiMPO_4$ is known as polaron-based [7] with electron or hole transfers along transition metal sites distorting the $LiMPO_4$ lattice. Particularly, these conductive particles are mainly and strongly localized on the M^{3+} sites in $Li_{1-x}MnPO_4$ during conduction. Thus, $LiMnPO_4$ shows a significantly lower electron conductivity (approximately, less than 1×10^{-10} S cm^{-1}) than the layer structured materials ($1 \times 10^{-3\sim5}$ S cm^{-1}) [2,8,9].

Tremendous efforts have been made to overcome this serious problem. Carbon coating is one of the useful methods for improving the electron conductivity on the surface of the active materials of $LiMPO_4$ [10–14]. The authors have already reported that $LiMnPO_4$ particles synthesized via the sol–gel method and carbon-coated by ball milling exhibited a higher specific capacity and rate property of over 120 mAh g^{-1} at 0.05 C and 100 mAh g^{-1} at 5 C, respectively [13]. Bakenov et al. reported that compounds of $LiMnPO_4$ and carbon were prepared by a spray pyrolysis method, thus leading to values of 153 mAh g^{-1} at 0.1 C and 80 mAh g^{-1} at 5 C [14].

* Corresponding author. Tel./fax: +81 559979824.
E-mail addresses: j.yoshi@fh.tec.toyota.co.jp, noblesseoblige1426@gmail.com (J. Yoshida).

0378-7753/$ – see front matter
http://dx.doi.org/10.1016/j.jpowsour.2012.09.081

On the other hand, some trials have been done to achieve higher lithium ion diffusion conductivity by using nanosized particles. Martha et al. reported that about 30 nm $LiMnPO_4$ particles, which were synthesized by a polyol method and carbon-coated by ball milling, showed good battery properties (145 mAh g^{-1} at 0.05 C and 70 mAh g^{-1} at 5 C) [15]. Drezen et al. [16] systematically investigated the relation between the particle size of $LiMnPO_4$ calculated from the specific surface area (BET) and the resultant battery properties. As a result, it was found that the best battery characteristic was obtained with a particle size of 140 nm. However, the size effect of the $LiMnPO_4$ particles on the battery's properties still remained unclear. To obtain a better insight into this subject, direct microscopic observations of the lithium behavior through the insertion/extraction reactions in the particles during the charge–discharge process will be very a powerful technique.

This paper will discuss the effect of the $LiMnPO_4$ particle size on the battery properties by introducing STEM-EELS, which is expected to allow for the direct microscopic observations of the lithium state in the particles during the charge-discharge process. Sol–gel and hydrothermal synthesis routes were selected to obtain differently sizes of the $LiMnPO_4$ particles.

2. Experimental

2.1. Synthesis of $LiMnPO_4$ powders

2.1.1. Sol–gel method

$LiMnPO_4$ powder ranging from a 50 nm to 200 nm particle size was prepared by the sol–gel method [17]. Fig. 1 is a flow chart of the sol–gel method. A stoichiometric ratio of $Li(CH_3COO)\cdot 2H_2O$ (Nacalai Tesque), $Mn(CH_3COO)_2\cdot 4H_2O$ (Nacalai Tesque, 99%), $HN_4H_2PO_4$ (Nacalai Tesque, 98%) and glycolic acid (Nacalai Tesque, 98%) was adjusted as the raw materials, and they were dissolved in distilled water. The amount of glycolic acid was five times the molar mass for the stoichiometry of $LiMnPO_4$ in order to avoid particle growth. The pH of the mixture was adjusted to about 1.5 by adding conc. nitric acid and kept constant during the sol–gel reaction. This solution was evaporated at 80 °C in an oil bath overnight while stirring. The obtained dark green gel was calcined at 120–200 °C for 5 h under ambient conditions to prepare the particles. The synthesized particles were then coated with carbon to improve the electron conductivity. The coating procedure will be explained in Section 2.1.3.

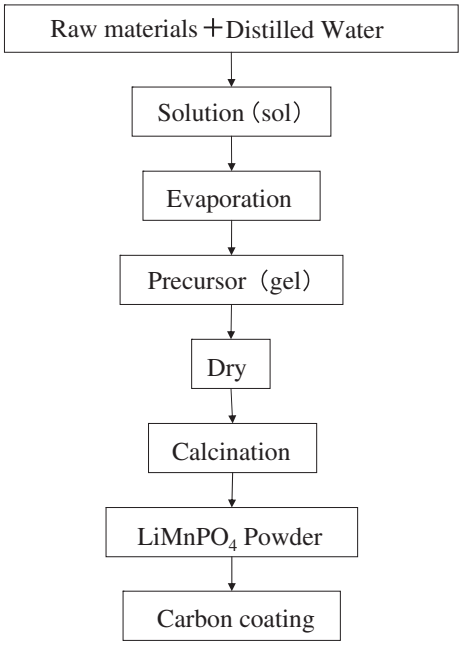

Fig. 1. Flow chart of sol–gel method for $LiMnPO_4$ powder.

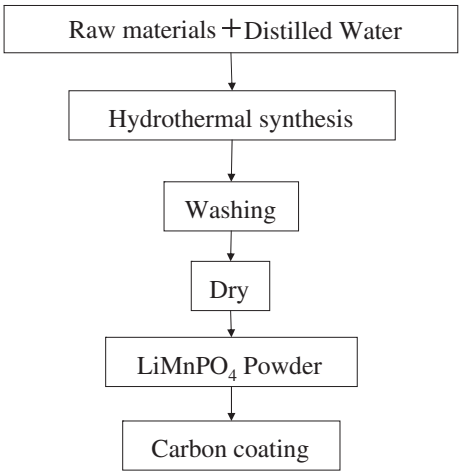

Fig. 2. Flow chart of hydrothermal synthesis method for $LiMnPO_4$ powder.

2.1.2. Hydrothermal synthesis

$LiMnPO_4$ powder, ranging from 20 nm to 50 nm, was prepared by a hydrothermal synthesis [18,19]. The synthesis is schematically shown in the flow chart of Fig. 2. Two precursor solutions prepared as follows were used to obtain the pure phase $LiMnPO_4$. Phosphoric acid (MERCK, 85%) and Triton H-66 (DOW Chemical) of 0.59 g and 7.5 g, respectively, were slowly added to distilled water using a syringe. $LiNO_3$(MERCK, 98%) and $MnNO_3\cdot 4H_2O$ (MERCK) of 6.89 g and 4.00 g, respectively, were then dissolved in the solution at 90 °C in an oil bath (solution 1).

For the second solution, 0.71 g of LiOH (Sigma–Aldrich, 98%) was dissolved in 10 g of distilled water (solution 2). Solution 2 was poured into solution 1 and mixed by a magnetic stirrer. After several hours, 0.71 g of glycine (MERCK) and a few drops of hydrazine monohydrate (MERCK) were added to both mixed solutions and stirred in the oil bath at 80 °C. The obtained solution was transferred in an autoclave, which was heated to 150 °C for 20 h while stirring the solution. The final precipitated product was washed with distilled water, ethanol and acetone. The washed particles were completely dried at 60 °C in an oven for about 12 h. The powder was also coated with carbon as described in Section 2.1.3.

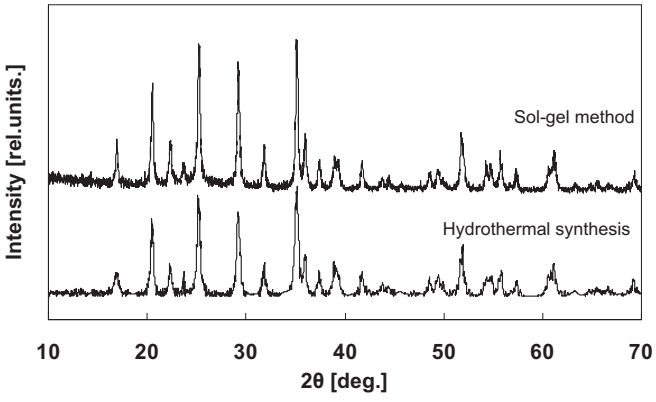

Fig. 3. XRD patterns of carbon-coated $LiMnPO_4$ particles synthesized by sol–gel method and hydrothermal synthesis.

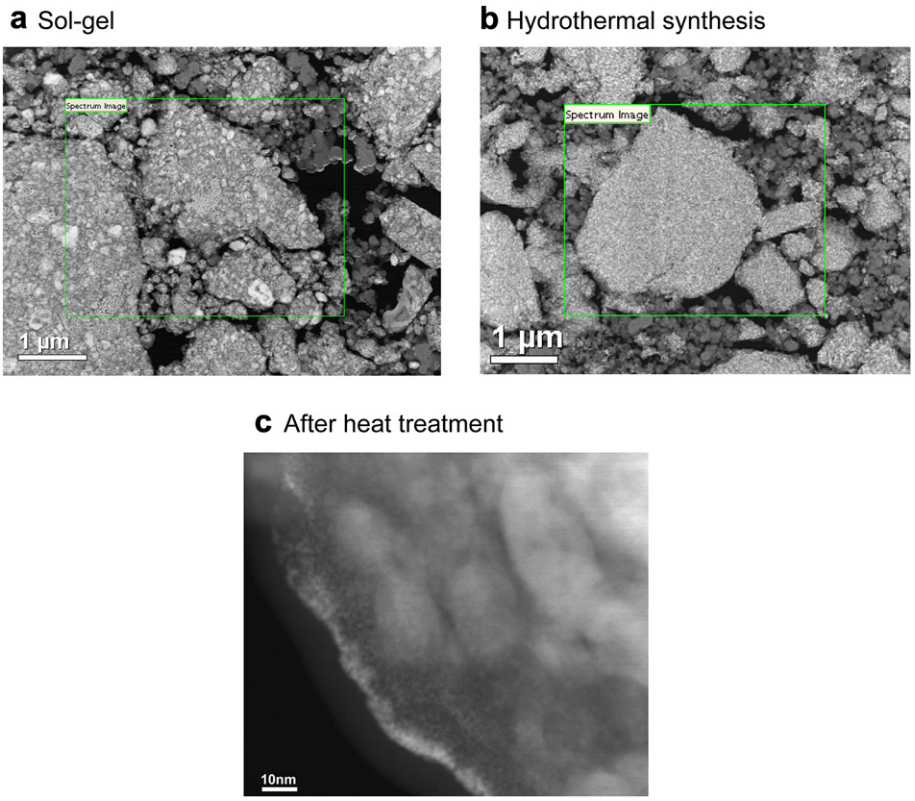

Fig. 4. STEM images of $LiMnPO_4$ particles coated carbon synthesized by (a) sol–gel method and (b) hydrothermal synthesis. (c) And (d) are high magnification image of hydrothermal synthesized sample. (c) The sample after heat treatment.

2.1.3. Carbon coating

The $LiMnPO_4$ particles made by both synthesis protocols were surface carbon-coated by ball milling. The $LiMnPO_4$ particles were first milled in a zirconia pot at 300 rpm for 3 h, and then 20 mass% of ketjen black (ECP-600JD, KB International) was added to for the $LiMnPO_4$. The mixture was processed at 300 rpm for 25 h. The obtained compounds were then annealed at 600 °C in an Ar atmosphere to crystallize the carbon-coated $LiMnPO_4$ olivine structure.

2.2. Material characterization

2.2.1. Electrochemical measurements

Electrodes were fabricated by the doctor blade method. The slurry was composed of the carbon-coated $LiMnPO_4$ material, acetylene black (HS-100, Denki kagaku kogyou), and PVdF (#9305, Kureha), whose mass ratio was 75:20:5. Its viscosity was adjusted by adding NMP (Nacalai Tesque, 98%). The slurry was then cast on Al foil and dried at 120 °C for 12 h in vacuum to make the film. The obtained electrodes were stamped out as disks of 16 mm diameter, and pressed a bulk density of 1.5–1.7 g cm^{-3} in a 5-ton press machine to obtain.

2.2.2. Morphology characterization

The microstructure of the electrode samples in a coin cell, such as the shape and size of the particles, was observed using an STEM (HD-2700, Hitachi High-Technologies Corporation). The electrode samples were thinned by FIB for observing their internal microstructure. The sample preparation was conducted in an air-free condition to avoid reactions with H_2O or oxygen in the air on the

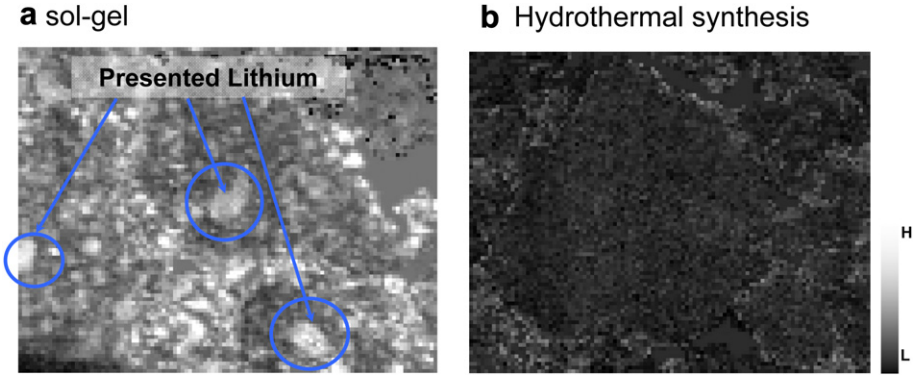

Fig. 5. Li-EELS mapping images of $LiMnPO_4$ prepared by (a) sol–gel method and (b) hydrothermal synthesis. These electrodes were amply charged in CC-CV mode at 0.05 C.

surface of the $LiMnPO_4$. The thinned specimens of the charged electrodes were electrochemically lithium extracted in the coin cells at a CC-CV charge of 0.05 C for 35 h. The charged electrodes were removed from the cells and rinsed three times with DMC in order to remove the electrolyte salt prior to the FIB. All experiments were carried out in an Ar glove box. The lithium distribution in the $LiMnPO_4$ particles of the charged electrodes was then directly analyzed by EELS (Electron Energy-loss spectroscopy). The lithium spectra from 50 eV to 100 eV were obtained, because the Li K-edge is situated at 60 eV. As the peak of the Li K-edge was really close to that of the Mn $M_{2,3}$-edge, an energy resolution of less than 0.2 eV was used. A scanning analysis was implemented to prepare the lithium maps of the particles and visualize the inactive parts during the charging.

3. Results and discussion

Fig. 3 shows the XRD patterns of the carbon-coated $LiMnPO_4$ particles synthesized by the sol–gel method and hydrothermal synthesis. All peaks were identified according to the olivine structure type in the space group Pnma. No impurity phases were found. When impurity phases exist, the peak of XRD associated with Li_3PO_4 appears between 22.4° and 23.8°. However, such peak was not detected as shown in Fig. 3.

Fig. 4(a) and (b) shows the corresponding STEM images of the fully charged samples prepared by the sol–gel and hydrothermal synthesis, respectively. Both samples were scraped from the electrode by FIB prior to the microscopic observations. Fig. 4(a) shows the sample made by the sol–gel method. Large agglomerates with sizes ranging from 1 to 10 μm composed of primary particles ranging from 10 nm to 150 nm were observed. In contrast, the hydrothermally synthesized powder as shown in Fig. 4(b) had large agglomerates in which nano-sized particles were closely packed. Fig. 4(c) shows a higher magnification STEM image of the largest agglomerate shown in Fig. 4(b). It is clearly visible that the primary particle size in the agglomerate is about 40 nm, and its size distribution is relatively uniform.

Fig. 5(a) and (b) show Li mapping images visualized by the EELS microscopic analysis. They were obtained by scanning within the square area shown in the STEM images of Fig. 4(a) and (b), respectively. The EELS spectrum of the Li K-edge exists around 60 eV. When the Li K-edge peak was detected, bright white features appeared in these images. On the contrary, the black parts show no residual lithium ions in the particles. As already mentioned, these samples were processed electrochemically in the CC-CV charge mode for 35 h at 0.05 C. However, in the sol–gel sample, the white features revealed that lithium ions still remained in the agglomerate as shown in Fig. 5(a). It is assumed that they were probably the inactive portion of the $LiMnPO_4$ particles during the electrochemical lithium insertion/extraction, and they would show an unexpected resistivity of the active material. Since $LiMnPO_4$ has a poor rate characteristic, it is important to clarify such inactive portions in order to obtain better battery properties.

On the contrary, very few white features were observed in the sample obtained by the hydrothermal approach as shown in Fig. 5(b). This clearly indicated that lithium ions could be extracted from the $LiMnPO_4$ particles of 40 nm size as shown in Fig. 4(c), even if the space filled with the electrolyte is very small inside the agglomerate. It suggests that smaller primary particles play an important role in improving the electrochemical properties, thus leading to an enhanced lithium ion extraction reaction.

Fig. 6 shows the EELS mapping images and the STEM image in which the primary particles were clearly observed in the sol–gel sample. The left square is located near the surface of a single agglomerate, and the right square is located in the center. Many primary particles are distributed in the agglomerate, ranging from 50 to 400 nm. Each primary particle has small pores. They were probably formed by gas evolution generated from organic materials such as acetate or glycolic acid in the primary particles during their calcination.

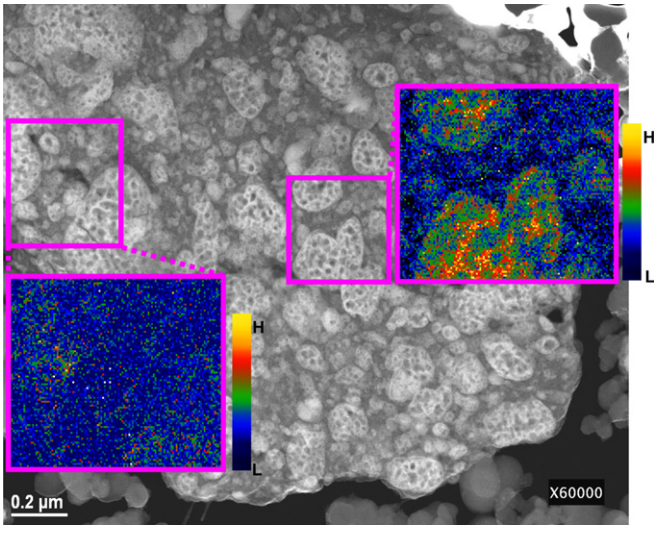

Fig. 6. STEM image of the $LiMnPO_4$ secondary particle charged in CC-CV mode at 0.05 C. Insets show the Li-EELS maps measured in the part enclosed with the square.

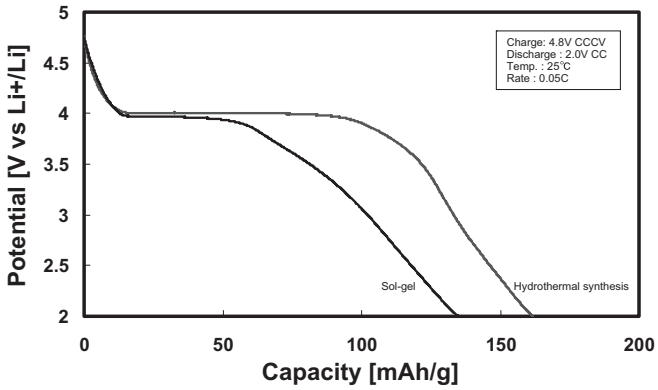

Fig. 7. Discharge curves of LiMnPO4 synthesized by each method.

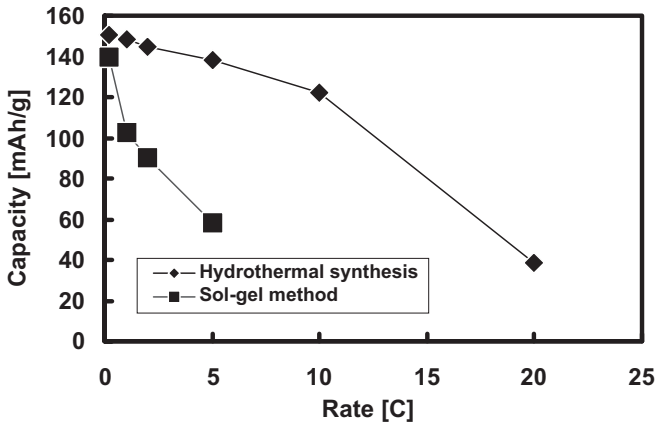

Fig. 8. Rate performance of $LiMnPO_4$ synthesized by each method.

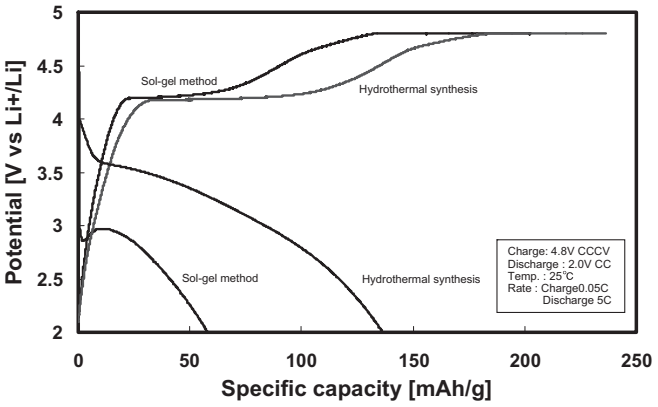

Fig. 9. Charge–discharge curves of $LiMnPO_4$ synthesized by each method. Both samples were charged at 0.05 C in CC-CV mode, and discharged at 5 C.

The colored dots in the EELS maps inset of Fig. 6 show the presence of lithium. In the surface region, a small number of dots exists, which means almost all of the lithium ions were extracted from this region after the electrochemical delithiation. On the contrary, many dots are observed in the primary particles in the center of the agglomerate. A lot of residual lithium ions still remained in this region. There differences clarified that the electrochemical reaction is limited by electrolyte penetration into the agglomerates. Nevertheless, lithium ions were removed from the smaller primary particles of 40 nm when they were located inside closely packed agglomerate structure as shown in Fig. 5(b). This is because the lithium ion conductivity would become higher due to a shorter conductive pass and large specific surface area, which would enhance the reaction activity between the active material and electrolyte. It is considered that the electrochemical reaction progressed by using small particles if the electrolyte contacts the surface of the primary particles. This will lead to the diffusion of lithium ions from inside of the particles to their surface.

The distance needed to transfer lithium ions from the inside to the surface of the single particles was measured by the EELS line analysis. It was carried out from the primary particle surface to its inside. As a result, almost all of lithium ions were removed from the point whose distance was less than 20 nm in the primary particle. In order to use all the lithium ions in the $LiMnPO_4$ particles during the electrochemical reaction, it is necessary to use smaller sized powders, although the C rate must be considered. The primary particle sizes available by the hydrothermal synthesis approach would probably satisfy the size range.

Fig. 7 shows the discharge curves of the samples used for the EELS analysis after charging in the CC-CV mode at 0.05 C. The specific capacity of the sample made by the sol–gel method was 135 mAh g^{-1}, while that made by the hydrothermal synthesis was 160 mAh g^{-1} which achieved 94% of the theoretical capacity. This result is ascribed to the full extraction of lithium from the primary particles observed by the STEM-EELS analysis as shown in Fig. 5(b).

Fig. 8 shows the rate properties of these samples. The rate capacity of the sample prepared by the hydrothermal synthesis was highly improved compared to that made by the sol–gel method. Especially, the specific capacity of the sample made by the hydrothermal synthesis was 136 mAh g^{-1} at 5 C and 120 mAh g^{-1} at 10 C, which are higher values when compared to those obtained by other reports [15,20]. This suggests that lithium ion diffusion into the particles of sizes less than 40 nm is improved during discharge.

As shown in Fig. 9, the battery resistivity of the $LiMnPO_4$ made by the hydrothermal synthesis was clearly lower than that made by the sol–gel method. However, the 5 C discharge profile shows that the polarization was still high, and that the average discharge voltage was lower compared to that obtained at 0.05 C. This suggests that this material still has a problem for use in practical cells of hybrid vehicles. A further study will be done to obtain a higher rate capability applicable for practical battery use.

4. Conclusions

Nano-sized $LiMnPO_4$ particles were synthesized via the sol–gel method and hydrothermal synthesis. XRD patterns of the prepared samples were identified as the olivine-type structure indexed by space group Pnma. The morphology, such as shape and particle size, was quite different depending on the synthesis process. The particle size of the sol–gel sample widely ranged from about 10 nm to 150 nm. On the other hand, the hydrothermally synthesized samples exhibited sizes of about 40 nm with a uniform size distribution. With the EELS analysis, it was clarified that the lithium diffusion distance from the inside to the surface of the primary particles had to be reduced down to about 20 nm. The hydrothermally synthesized samples realized this condition and exhibited 160 mAh g^{-1} at 0.05 C and 136 mAh g^{-1} at 5 C. EELS mapping images clarified that the application of nano-sized $LiMnPO_4$ particles effectively improved the battery properties due to shortening of the lithium ion diffusion path.

References

[1] A.K. Padhi, K.S. Nanjundaswamy, J.B. Goodenough, Journal of Electrochemical Society 144 (1997) 1188–1194.
[2] M. Yoneyama, A. Yamada, Y. Takei, N. Sonoyama, R. Kanno, Journal of Electrochemical Society 151 (9) (2004) A1352–A1356.
[3] A. Yamada, M. Hosoya, S.-C. Chung, Y. Kudo, K. Hinokuma, K.-Y. Liu, Y. Nishi, Journal of Power Sources 119–121 (2003) 232–238.
[4] C. Delacourt, L. Laffont, R. Bouchet, C. Wurm, J.-B. Leriche, M. Morcrette, J.-M. Tarascon, C. Masquelier, Journal of Electrochemical Society 152 (5) (2005) A913–A921.
[5] J.-W. Lee, M.-S. Park, B. Anass, J.-H. Park, M.-S. Paik, S.-G. Doo, Electrochimica Acta 55 (2010) 4162–4169.
[6] T. Shiratsuchi, S. Okada, T. Doi, J. Yamaki, Electrochimica Acta 54 (2009) 3145–3151.
[7] K. Zaghib, A. Mauger, J.B. Goodenough, F. Gendron, C.M. Julien, Chemistry of Materials 19 (2007) 3740–4374.
[8] H. Tukamoto, A.R. West, Journal of Electrochemical Society 144 (1997) 3164–3168.
[9] J. Molenda, P. Wilk, J. Marzec, Solid State Ionics 146 (2002) 73–79.
[10] J. Yang, J.J. Xu, Journal of Electrochemical Society 153 (2006) A716–A720.
[11] H. Joachin, T.D. Kaun, K. Zaghib, J. Parkash, Journal of Electrochemical Society 156 (6) (2009) A401–A406.
[12] Y.-D. Cho, G.T.-K. Fey, H.-M. Kao, Journal of Power Sources 189 (2009) 256–262.
[13] J. Yoshida, S. Nakanishi, H. Iba, H. Abe, M. Naito, Journal of the Society of Powder Technology, Japan 48 (2011) 389–395.
[14] Z. Bakenov, I. Taniguchi, Journal of Power Sources 195 (2010) 7445–7451.
[15] S.K. Martha, B. Markovsky, J. Grinblat, Y. Gofer, O. Haik, E. Zinigrad, D. Aurbach, T. Drezen, D. Wang, G. Deghenghi, I. Exnar, Journal of Electrochemical Society 156 (7) (2009) A541–A552.
[16] T. Drezen, N.-H. Kwon, P. Bowen, I. Teerlinck, M. Isono, I. Exnar, Journal of Power Sources 174 (2007) 949–953.
[17] J. Yoshida, S. Nakanishi, H. Iba, H. Abe, M. Naito, Journal of the Society of Powder Technology, Japan 48 (2011) 473.
[18] J. Yoshida, N. Sato, N. Huesing, M. Stark, PCT IB2009-000306 (Filed February 2009, issued August 2010).
[19] M. Stark, Q. Liu, A. Chuvilin, J. Yoshida, N. Sato, T. Saito, U. Kaiser, N. Husing, MRS fall meeting, Boston (MA), USA, 2010.
[20] T.N.L. Doan, I. Taniguchi, Journal of Power Sources 196 (2011) 1399–1408.